NMR studies of the incommensurate helical antiferromagnet $EuCo_2P_2$: Determination of antiferromagnetic propagation vector

Nonoka Higa,[1,2] Qing-Ping Ding,[1] Mamoru Yogi,[2] N. S. Sangeetha,[1] Masato Hedo,[2] Takao Nakama,[2] Yoshichika Ōnuki,[2] D. C. Johnston,[1] and Yuji Furukawa[1]

[1]*Ames Laboratory, U.S. Department of Energy, and Department of Physics and Astronomy, Iowa State University, Ames, Iowa 50011, USA*

[2]*Department of Physics and Earth Sciences, Faculty of Science, University of the Ryukyus, Okinawa 903-0213, Japan*

(Received 27 April 2017; revised manuscript received 15 June 2017; published 6 July 2017)

Recently, Q.-P. Ding *et al.* [Phys. Rev. B **95**, 184404 (2017)] reported that their nuclear magnetic resonance (NMR) study on $EuCo_2As_2$ successfully characterized the antiferromagnetic (AFM) propagation vector of the incommensurate helix AFM state, showing that NMR is a unique tool for determination of the spin structures in incommensurate helical AFMs. Motivated by this work, we have carried out ^{153}Eu, ^{31}P, and ^{59}Co NMR measurements on the helical antiferromagnet $EuCo_2P_2$ with an AFM ordering temperature $T_N = 66.5$ K. An incommensurate helical AFM structure was clearly confirmed by ^{153}Eu and ^{31}P NMR spectra on single-crystalline $EuCo_2P_2$ in zero magnetic field at 1.6 K and its external magnetic field dependence. Furthermore, based on ^{59}Co NMR data in both the paramagnetic and incommensurate AFM states, we have determined the model-independent value of the AFM propagation vector $\mathbf{k} = (0,0,0.73 \pm 0.09)2\pi/c$, where c is the c-axis lattice parameter. The temperature dependence of $\mathbf{k}$ is also discussed.

DOI: 10.1103/PhysRevB.96.024405

I. INTRODUCTION

A great deal of attention in studying magnetism has been given to systems with geometric frustration [1,2]. Such competing magnetic interactions between localized spins often result in noncollinear magnetic structures, such as incommensurate helical magnetic structures. Usually, such noncollinear magnetic structures are determined by using neutron diffraction (ND) measurements.

Very recently, nuclear magnetic resonance (NMR) was shown to be another unique tool to determine spin structures in incommensurate helical antiferromagnets (AFMs) [3]. By performing ^{153}Eu, ^{75}As, and ^{59}Co NMR measurements on the incommensurate helical AFM $EuCo_2As_2$ with an ordering temperature $T_N = 45$ K, the AFM propagation vector of the incommensurate helical AFM state was successfully determined [3]. Such an NMR approach can be used to characterize the magnetic structure in other possible helical magnets such as the isostructural metallic compound $EuCo_2P_2$ [4] and $EuCu_{1.82}Sb_2$ [5].

Motivated by the above NMR work, we have carried out NMR measurements to characterize $EuCo_2P_2$ with the body-centered tetragonal $ThCr_2Si_2$-type structure which is reported to exhibit an incommensurate helical AFM ground state below $T_N = 66.5$ K [4,6–9]. The neutron diffraction measurements [4] on $EuCo_2P_2$ report that the Eu ordered moment at 15 K is $6.9\mu_B$/Eu, where μ_B is the Bohr magneton, consistent with Eu^{2+} ($J = S = 7/2$) and spectroscopic splitting factor $g = 2$. The magnetic structure is the same as that in $EuCo_2As_2$ [10], where the Eu ordered moments are aligned ferromagnetically in the ab plane with the helix axis along the c axis [4]. The AFM propagation vector $\mathbf{k} = (0,0,0.852)2\pi/c$ at 15 K was determined by the ND measurements [4], where c is the c-axis lattice parameter. A similar value of $\mathbf{k} = (0,0,0.88)2\pi/c$ at $T = 0$ K (Ref. [9]) was also obtained through the analysis of χ data on a single crystal below T_N using molecular field theory, which has been recently formulated to apply to planar noncollinear Heisenberg antiferromagnets [11–13]. It is important to independently determine the AFM propagation vector $\mathbf{k}$ by using the NMR technique.

Another interesting feature of metallic $EuCo_2P_2$ is a change in magnetic properties observed under high pressure [14]. With the application of pressure, $EuCo_2P_2$ exhibits a first-order tetragonal to collapsed-tetragonal transition and an associated valence transition from Eu^{2+} to nonmagnetic Eu^{3+} ($J = 0$) at 3.1 GPa. Below 3.1 GPa, the AFM ordering originates from Eu $4f$ local moments where Co moments are considered not to be involved in the magnetic ordering. On the other hand, above 3.1 GPa, the change in the Eu valence from 2+ to 3+ leads to the appearance of itinerant $3d$ magnetic ordering below 260 K. Thus, it is interesting and important to characterize the magnetic and electronic states of each ion in $EuCo_2P_2$ from a microscopic point of view.

In this paper, we report NMR results on $EuCo_2P_2$, where we succeeded in observing NMR signals from ^{153}Eu, ^{59}Co, and ^{31}P nuclei, focusing our attention on the spin structure in the incommensurate helical AFM state with the aim of obtaining better understanding of the local magnetic and electronic properties of the three ions in the AFM and paramagnetic states at ambient pressure. From the external field dependence of ^{153}Eu and ^{31}P NMR spectra at 1.6 K, below $T_N = 66.5$ K an incommensurate helical AFM state shown in Fig. 1 was clearly evidenced in $EuCo_2P_2$. Furthermore, the AFM propagation vector characterizing the helical AFM state is determined to be $\mathbf{k} = (0,0,0.73 \pm 0.09)2\pi/c$ from the internal magnetic induction at the Co site obtained with ^{59}Co NMR under zero magnetic field. The estimated value is slightly smaller than those reported from the neutron diffraction and magnetic susceptibility measurements [4,9]. ^{59}Co NMR revealed that no magnetic ordering of the Co $3d$ electron spins occurs in the helix AFM state, evidencing that the magnetism in $EuCo_2P_2$ originates from only the Eu spins. The temperature dependence of the Eu ordered moments determined by the internal magnetic induction at the P site B_{int}^{P} can be well reproduced by the Brillouin function with $J = S = 7/2$, confirming that the magnetic state of the Eu^{2+} ions is well

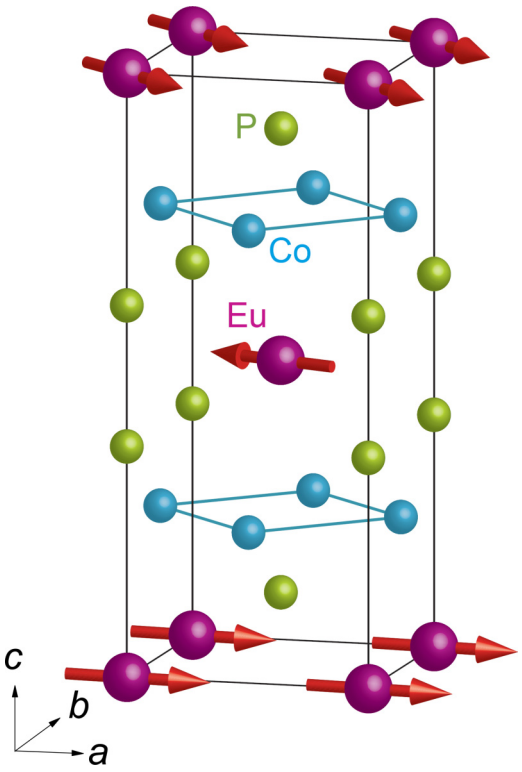

FIG. 1. Crystal and magnetic structures of $EuCo_2P_2$. The arrows on the Eu atoms indicate the directions of the Eu ordered moments in the incommensurate helical antiferromagnetic state.

explained by the local moment picture although the system is metallic. Our NMR study shows again that NMR is a powerful tool for determination of the spin structure in incommensurate helical AFMs.

II. EXPERIMENT

A single crystal ($1 \times 1 \times 0.3$ mm^3) of $EuCo_2P_2$ for the NMR measurements was grown using Sn flux [6,9]. NMR measurements of ^{153}Eu ($I = \frac{5}{2}$, $\frac{\gamma_N}{2\pi} = 4.632$ MHz/T, $Q = 2.49$ barns), ^{59}Co ($I = \frac{7}{2}$, $\frac{\gamma_N}{2\pi} = 10.03$ MHz/T, $Q = 0.4$ barns), and ^{31}P ($I = \frac{1}{2}$, $\frac{\gamma_N}{2\pi} = 17.235$ MHz/T) nuclei were conducted using a homemade phase-coherent spin-echo pulse spectrometer. In the AFM state, ^{153}Eu, ^{31}P, and ^{59}Co NMR spectra in zero and nonzero magnetic fields H were measured in steps of frequency f by measuring the intensity of the Hahn spin echo. We have used a single crystal for ^{153}Eu and ^{31}P NMR spectrum measurements at the lowest temperature of 1.6 K. Above $T = 1.6$ K, we performed our measurements using powdered single crystals as intensities of NMR signals with the single crystals were too weak to perform the measurements at higher temperatures. In the paramagnetic (PM) state, ^{59}Co and ^{31}P NMR spectra were obtained by sweeping the magnetic field at $f = 51.2$ MHz.

III. RESULTS AND DISCUSSION

A. ^{153}Eu NMR spectrum

The bottom panel of Fig. 2 shows the ^{153}Eu NMR spectrum in the AFM state for $EuCo_2P_2$ (single crystal) measured in zero magnetic field at a temperature $T = 1.6$ K. An almost identical ^{153}Eu NMR spectrum was observed on a powder sample $EuCo_2P_2$ at 1.6 K (not shown). The observed spectrum is well reproduced by the following nuclear spin Hamiltonian for the case where the Zeeman interaction is much greater than the quadrupole interaction, which produces a spectrum with a central transition line flanked by two satellite peaks on both sides for $I = 5/2$:

$$\mathcal{H} = -\gamma\hbar\mathbf{I}\cdot\mathbf{B}_{\rm int} + \frac{h\nu_Q}{6}\left[3I_z^2 - I(I+1) + \frac{1}{2}\eta(I_+^2 + I_-^2)\right], \tag{1}$$

where $B_{\rm int}$ is the internal magnetic induction at the Eu site, h is Planck's constant, and ν_Q is the nuclear quadrupole frequency defined by $\nu_Q = 3e^2QV_{ZZ}/2I(2I-1)h$ ($=3e^2QV_{ZZ}/20h$ for $I = 5/2$), where Q is the electric quadrupole moment of the Eu nucleus, V_{ZZ} is the electric field gradient (EFG) at the Eu site, and η is the asymmetry parameter of the EFG [15]. Since the Eu site in $EuCo_2P_2$ has a tetragonal local symmetry ($4/mmm$), η is zero. The red line shown in the bottom panel of Fig. 2 is the calculated spectrum for ^{153}Eu zero-field NMR (ZFNMR) using the parameters $|B_{\rm int}^{\rm Eu}| = 25.75(2)$ T ($=119.3$ MHz), $\nu_Q = 30.2(2)MHz$, and $\theta = 90^\circ$. Here θ represents the angle between $B_{\rm int}^{\rm Eu}$ and the principal axis of the EFG tensor at the Eu sites.

Since the principal axis of the EFG at the Eu site is parallel to the c axis due to the local symmetry [3,16], $\theta = 90^\circ$ indicates

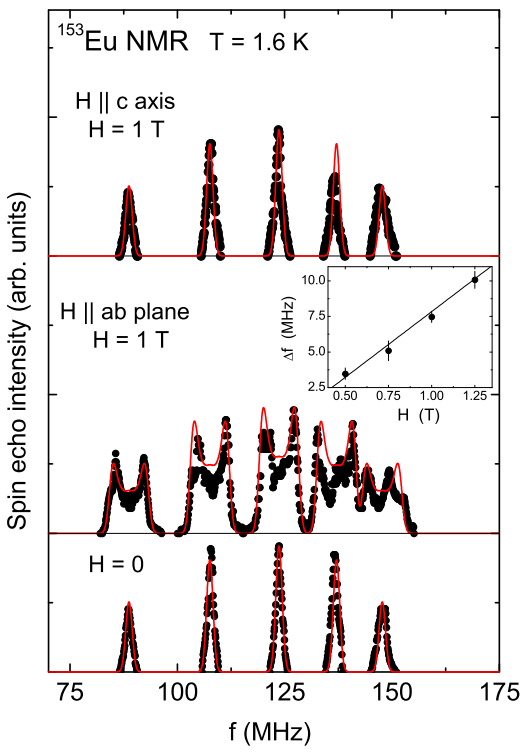

FIG. 2. ^{153}Eu NMR spectra at $T = 1.6$ K in the AFM state for single-crystalline $EuCo_2P_2$ in $H = 0$ (bottom panel) and $H = 1$ T parallel to the ab plane (middle panel) and parallel to the c axis (top panel). The red lines constitute the calculated ^{153}Eu NMR spectrum. The inset shows the external magnetic field dependence of the amount of splitting of the central transition line Δf. The solid line is the expected H dependence of Δf described in the text.

that $B_{\rm int}^{\rm Eu}$ is perpendicular to the c axis. This is similar to the case of the Eu nuclei in $EuCo_2As_2$ and $EuGa_4$ with the same $ThCr_2Si_2$-type crystal structure in which similar values of $B_{\rm int}^{\rm Eu} = 27.5$ and 27.08 T and $\nu_{\rm Q} = 30.6$ and 30.5 MHz for ^{153}Eu, respectively, have been reported [3,16]. $B_{\rm int}^{\rm Eu}$ is proportional to $A_{\rm hf}\langle\mu\rangle$, where $A_{\rm hf}$ is the hyperfine coupling constant and $\langle\mu\rangle$ is the ordered Eu magnetic moment. The hyperfine field at the Eu sites mainly originates from core polarization from $4f$ electrons and is oriented in a direction opposite that of the Eu moment [17]. For $|B_{\rm int}^{\rm Eu}| = 25.75(2)$ T and the reported AFM ordered moment $\langle\mu\rangle = 6.9(1)\,\mu_{\rm B}$/Eu from ND [4], $A_{\rm hf}$ is estimated to be -3.73 T/$\mu_{\rm B}$ where the sign is reasonably assumed to be negative due to the core-polarization mechanism. The estimated $A_{\rm hf}$ is very close to -3.78 T/$\mu_{\rm B}$ for the case of $EuCo_2As_2$ [3] and is not far from the core-polarization hyperfine coupling constant -4.5 T/$\mu_{\rm B}$ estimated for Eu^{2+} ions [17]. The small difference could be explained by a positive hyperfine coupling contribution due to conduction electrons which cancels part of the negative core polarization field, as has been pointed out in the case of $EuCo_2As_2$ (Ref. [3]).

The direction of $B_{\rm int}^{\rm Eu}$ is also directly confirmed by ^{153}Eu NMR spectrum measurements on the single crystal in nonzero H. When H is applied along the c axis, almost no change in the ^{153}Eu NMR spectrum is observed (see the top panel in Fig. 2, where the simulated spectrum shown by the red line is the same as the case with $H = 0$). Since the effective field at the Eu site is given by the vector sum of $\mathbf{B}_{\rm int}^{\rm Eu}$ and $\mathbf{H}$, i.e., $|\mathbf{B}_{\rm eff}| = |\mathbf{B}_{\rm int}^{\rm Eu} + \mathbf{H}|$, the resonance frequency is expressed for $H \perp \langle\mu\rangle$ as $f = \frac{\gamma_{\rm N}}{2\pi}\sqrt{(B_{\rm int}^{\rm Eu})^2 + H^2}$. For our applied field range where $B_{\rm int}^{\rm Eu} \gg H$, any shift in the resonance frequency due to H would be small, as observed. Thus, we conclude that H is perpendicular to $B_{\rm int}^{\rm Eu}$ and thus to the ordered Eu moments.

In the case of $\mathbf{H}$ applied parallel to the ab plane, on the other hand, each line broadens and exhibits the typical two-horn structure expected for an incommensurate planar helical structure, as shown in the middle panel of Fig. 2. In fact, the observed spectrum at $H = 1$ T is well reproduced by the calculated spectrum for an incommensurate helical AFM state shown by the red line. The inset in the middle panel of Fig. 2 shows the external field dependence of the amount of the splitting of the central transition line Δf of the ^{153}Eu ZFNMR spectra. Δf increases with increasing H. Since the peak positions of the two-horn shape of the spectrum are given by $B_{\rm eff} = B_{\rm int} \pm H$, Δf is proportional to H according to $\Delta f = 2H\gamma_{\rm N}/(2\pi)$. As shown by the solid line in the inset, the H dependence of Δf is well reproduced by this relation. Thus, these NMR results are consistent with an incommensurate helical spin structure with the ordered moments aligned along the ab plane as reported from the ND [4] and magnetization [9] measurements. The observed ab-plane alignment of the ordered moments is also consistent with the prediction of the moment alignment from magnetic dipole interactions between the Eu spins [18].

B. ^{31}P NMR spectrum

The incommensurate planar helix structure is also clearly evidenced by ^{31}P NMR measurements. The bottom panel of Fig. 3 shows the ^{31}P ZFNMR spectrum at 1.6 K in the AFM state, where the red line is the fit with the parameter $|B_{\rm int}^{\rm P}| = 2.69$ T. For $I = 1/2$, a single NMR line is expected and observed because of no quardupole interaction. When $\mathbf{H}$ is applied along the c axis, almost no change in the spectrum is observed, as shown in the top panel of Fig. 3, where $H = 0.1$ T. For comparison, we show the red line calculated for $H = 0$. This indicates that $\mathbf{H}$ is perpendicular to $\mathbf{B}_{\rm int}$ at the P site. On the other hand, when $\mathbf{H} = 0.1$ T is applied parallel to the ab plane, similar to the case of the ^{153}Eu NMR spectrum, the line exhibits a characteristic two-horn shape, again expected for the incommensurate planar helix AFM state.

As discussed for $EuGa_4$ (Ref. [16]) and $EuCo_2As_2$ (Ref. [3]), the direction of $B_{\rm int}^{\rm P}$ is antiparallel to the Eu ordered moments in the case where the Eu ordered moments are ferromagnetically aligned in the Eu plane, as shown in Fig. 4(a). Therefore, one can expect almost no change in the ^{31}P NMR spectrum when H is perpendicular to the Eu ordered moment, as observed in the ^{31}P NMR spectrum for $H \parallel c$ axis. On the other hand, if one applies $H \parallel ab$ plane, a splitting of the ^{31}P ZFNMR spectrum is expected, similar to the case of the ^{153}Eu ZFNMR spectrum. The red line in the middle panel of Fig. 3 is the calculated spectrum of ^{31}P NMR for the planar helix AFM structure under $H = 0.1$ T, which reproduces the observed spectrum very well.

The T dependence of the ^{31}P ZFNMR spectrum was measured up to 60 K. With increasing T, the spectra shift to lower frequency due to the reduction of the internal magnetic

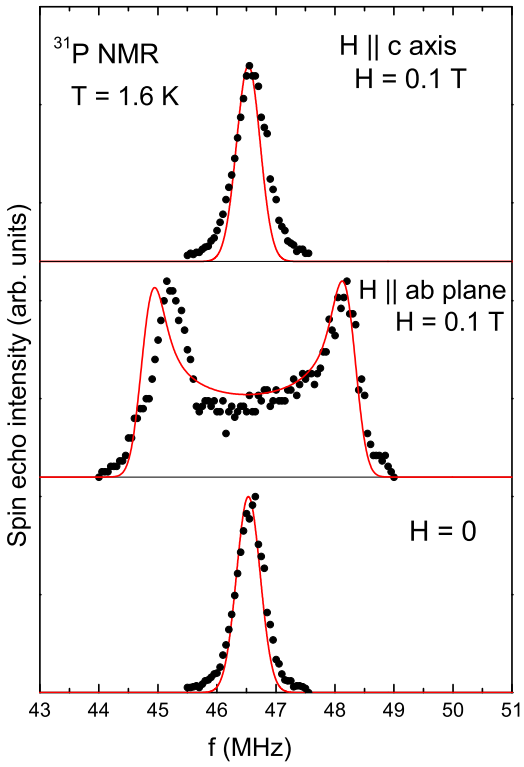

FIG. 3. ^{31}P NMR spectra at $T = 1.6$ K in the AFM state for $EuCo_2P_2$ in zero magnetic field (bottom panel) and under magnetic fields parallel to the ab plane (middle panel) and parallel to the c axis (top panel). The red lines are the calculated ^{31}P NMR spectra.

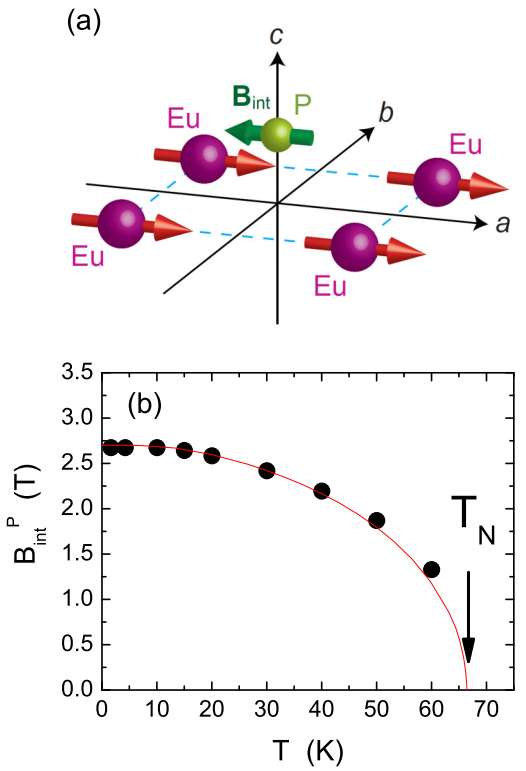

FIG. 4. (a) Coordination of nearest-neighbor Eu sites around a P site. The arrows on the Eu and P atoms indicate the directions of the Eu ordered moments and the internal magnetic induction at the P site, respectively. (b) Temperature dependence of $B_{\rm int}^{\rm P}$. The solid curve is the Brillouin function with $J = S = 7/2$.

induction $|B_{\rm int}^{\rm P}|$, which decreases from 2.69 T at 1.6 K to 1.33 T at 60 K. The T dependence of $|B_{\rm int}^{\rm P}|$ is shown in Fig. 4(b), which is the T dependence of the order parameter of the planar helix AFM state and is well reproduced by a Brillouin function which was calculated based on the Weiss molecular field model with $J = S = 7/2$, $T_{\rm N} = 66.5$ K, and $B_{\rm int}^{\rm P} = 2.69$ T at $T = 1.6$ K [solid curve in Fig. 4(b)]. This indicates that the magnetic state of the Eu ions is well explained by the local moment picture, although the system is metallic, as determined from electrical resistivity measurements [9].

Now we discuss our NMR data for the PM state. Figure 5 shows the temperature dependence of the field-swept ^{31}P NMR spectra for powdered single crystals and $T = 150$ to 300 K. With decreasing T, the peak position shifts to higher magnetic field, and the line becomes broader and asymmetric due to anisotropy in the Knight shifts in the powder sample. We determine the NMR shifts for H parallel to the c axis ($^{31}K_c$) and parallel to the ab plane ($^{31}K_{ab}$) from fits of the spectra shown by the red lines. The T dependences of $^{31}K_c$ and $^{31}K_{ab}$ are shown in Fig. 6. The hyperfine coupling constants $A^{\rm P}$ of ^{31}P surrounded by Eu^{2+} ions can be estimated from the slopes of K-χ plots with the relation

$$A = \frac{N_{\rm A}}{Z}\frac{K(T)}{\chi(T)}, \qquad (2)$$

where the $\chi(T)$ data are from Ref. [9], $N_{\rm A}$ is Avogadro's number, and $Z = 4$ is the number of nearest-neighbor (NN)

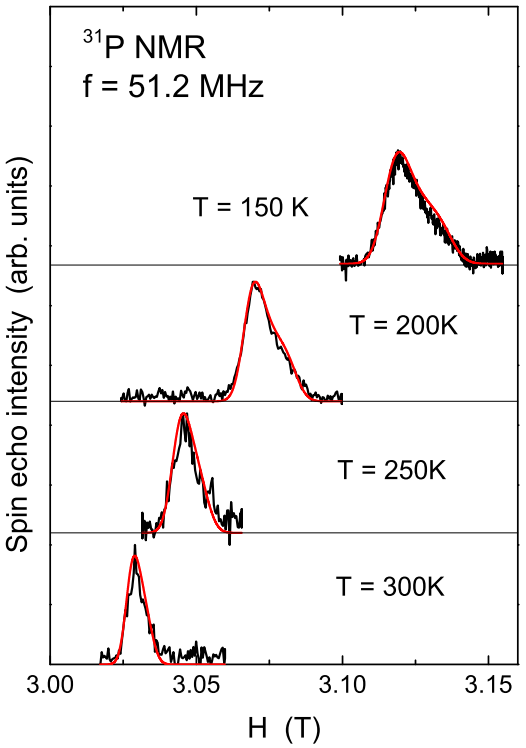

FIG. 5. Field-swept ^{31}P NMR spectra of $EuCo_2P_2$ (powder sample) measured at $f = 51.2$ MHz. The red lines are simulated spectra with hyperfine anisotropy.

Eu^{2+} ions around a P atom. Here we assume the hyperfine field at the P sites mainly originates from the NN Eu spins. As shown in the inset of Fig. 6, both $^{31}K_c$ and $^{31}K_{ab}$ vary linearly with χ. From the respective slopes, the hyperfine coupling constants $A_c^{\rm P}$ and $A_{ab}^{\rm P}$ are estimated to be -1.43 ± 0.10 and -1.23 ± 0.09 kOe/$\mu_{\rm B}$ per Eu, respectively.

With the value of $|B_{\rm int}^{\rm P}| = 2.69$ T, the Eu ordered moment is estimated to be $\langle\mu\rangle = 5.46\ \mu_{\rm B}$ at 1.6 K using the relation $|B_{\rm int}^{\rm P}| = 4A_{ab}^{\rm P}\langle\mu\rangle$. This value is smaller than $6.9\mu_{\rm B}$/Eu reported from the ND study [4]. The difference may suggest that the estimated $A_{ab}^{\rm P}$ in the PM state is slightly greater than

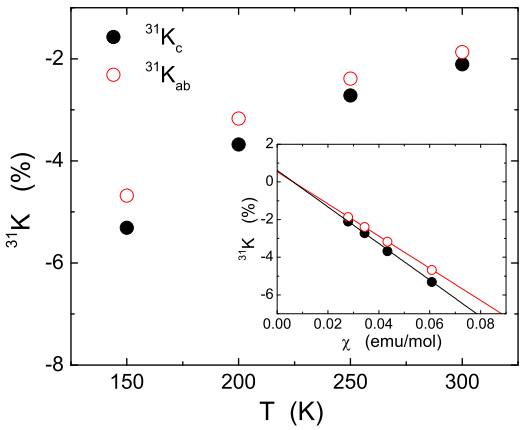

FIG. 6. Temperature dependences of the ^{31}P Knight shifts ^{31}K in the paramagnetic state. The inset shows $K(T)$ versus magnetic susceptibility $\chi(T)$. The solid lines are linear fits.

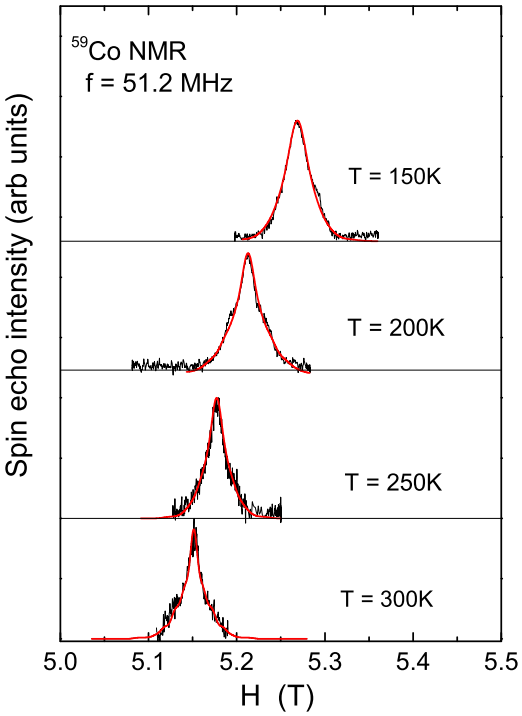

FIG. 7. Field-swept ^{59}Co NMR spectra in the paramagnetic state of $EuCo_2P_2$ (powder sample) measured at $f = 51.2$ MHz.

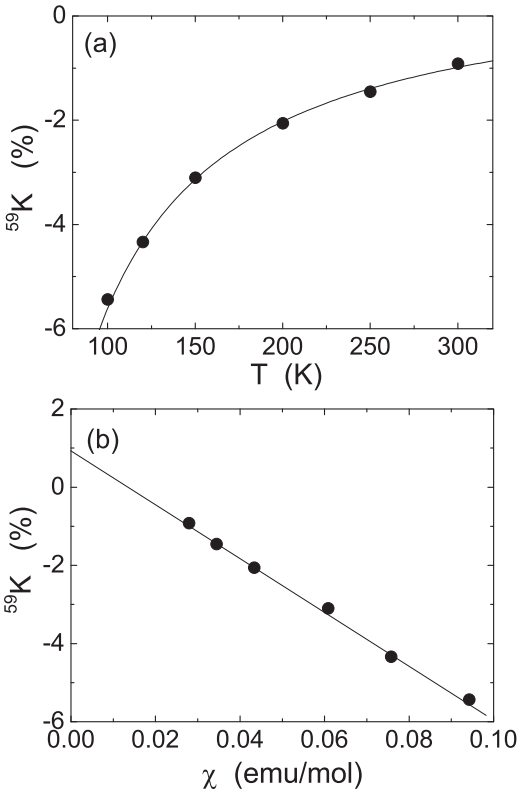

FIG. 8. (a) Temperature dependence of ^{59}Co Knight shift ^{59}K in the paramagnetic state. The solid line is fit to the data by a Curie-Weiss law. (b) $K(T)$ versus magnetic susceptibility $\chi(T)$. The solid line is a linear fit.

that in the AFM state. This would be possible if one took finite contributions to hyperfine fields from the next-nearest-neighbor (NNN) Eu spins on the next layer into consideration. Since in the AFM state the direction of NNN Eu spins is antiparallel to that of the NN Eu spins, one expects a positive hyperfine field at the P sites, which cancels part of the negative hyperfine field produced by the NN Eu spins. Assuming $\langle\mu\rangle = 6.9\mu_B$ (Ref. [4]), we thus estimate an ~21% net additional contribution to the hyperfine field from the NNN Eu spins.

C. ^{59}Co NMR spectrum

Figure 7 shows the temperature dependence of the field-swept ^{59}Co NMR spectra in the PM state of a powder sample where the spectra are seen to broaden with decreasing T. Although one expects a central transition line with three satellite lines on both sides for $I = 7/2$ nuclei, the observed spectra do not show the seven peaks but rather exhibit a single broad line due to inhomogeneous magnetic broadening. Since the powder sample consists of grains with randomly oriented crystal axes, the spectra are powder patterns. From the fitting of the spectra shown by red lines which are calculated from the nuclear spin Hamiltonian with a Zeeman interaction much greater than the quadrupole interaction, we estimate $\nu_Q \sim 0.25$ MHz, which is nearly independent of T. The broadening of the spectra with lowering T originates from magnetic broadening. The T dependence of the NMR shift ^{59}K determined from the peak position of the spectrum is shown in Fig. 8(a), where we fit the data with the Curie-Weiss law $\frac{C}{T-\theta_p}$. The solid line is a fit with $C = -533(13)\%$ K and $\theta_p = 18(3)$ K for ^{59}K. The value $\theta_p = 18(3)$ K is the same, within error, as the powder averaged value obtained for a single crystal of $EuCo_2P_2$ from $\chi(T)$ measurements [9]. The positive value of θ_p indicates predominant ferromagnetic (FM) exchange interactions between the Eu spins. This is consistent with the in-plane FM exchange interactions responsible for the planar helix AFM structure. The hyperfine coupling constant A^{Co} for ^{59}Co surrounded by $Z = 4$ Eu^{2+} ions is also estimated from the slope of the K-χ plot in Fig. 8(b) with Eq. (2). We thus estimate $A^{Co} = (-0.98 \pm 0.09)$ kOe/μ_B per Eu. This value is much smaller than a typical value $A = -105$ kOe/μ_B for Co $3d$ electron core polarization [17]. This indicates that the hyperfine field at the Co site originates from the transferred hyperfine field produced by the Eu spins and that no $3d$ spins on the Co sites contribute to the magnetism of $EuCo_2P_2$.

We now consider the influence of the planar helix AFM state on the Co NMR data. We tried to detect the signals in the AFM state using a single crystal, but we could not find any. Then we used powder samples, for which we succeeded in observing the ^{59}Co ZFNMR spectrum up to 30 K, as shown in Fig. 9. From the peak position of the spectrum, the internal magnetic induction at the Co site at 1.6 K is estimated to be $|B_{int}^{Co}| = 11.3$ kOe, which decreases to 10.2 kOe at 30 K. According to the analysis performed in $EuCo_2As_2$ [3], one can estimate the AFM propagation vector in the incommensurate state of $EuCo_2P_2$ based on the estimated values of $|B_{int}^{Co}|$ and A^{Co}. Here we present a discussion similar to that in [3].

In an incommensurate helical AFM state, $|B_{int}|$ at the Co site appears only in the ab plane when the Eu ordered moments

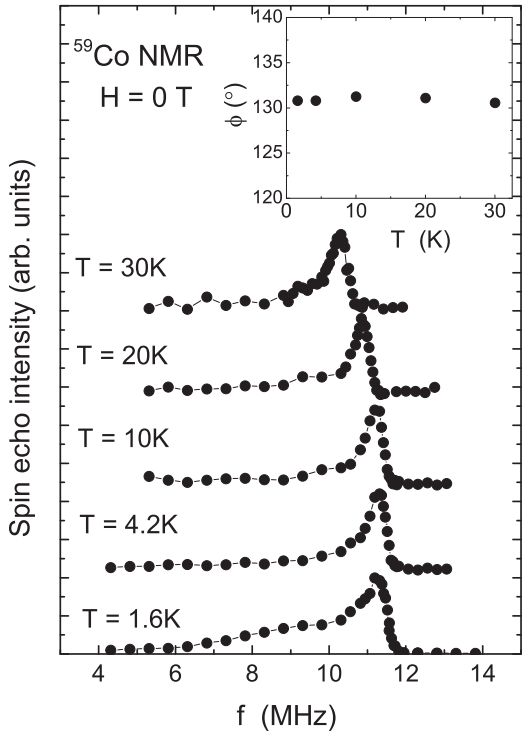

FIG. 9. ^{59}Co zero-field NMR spectra in the AFM state in zero magnetic field at the indicated temperatures. The inset shows the temperature dependence of the turn angle ϕ.

lie in the ab plane and is expressed by [3]

$$B_{\rm int}^{\rm Co} = 2\langle\mu\rangle A^{\rm Co}\sqrt{2+2\cos\phi}, \tag{3}$$

where ϕ is the turn angle along the c axis between the Eu ordered moments in adjacent Eu planes, which characterizes the helical structure. In the case of $\phi = \pi$, corresponding to a collinear AFM state, $B_{\rm int}^{\rm Co}$ is zero due to a cancellation of the internal magnetic induction from the four nearest-neighbor Eu ordered moments. On the other hand, if ϕ deviates from π, corresponding to a helical state, one can expect a finite $B_{\rm int}^{\rm Co}$ [see Fig. 10(a)]. Thus, the observation of the finite $B_{\rm int}^{\rm Co}$ is

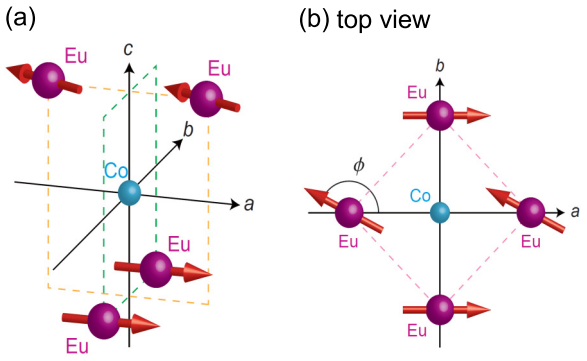

FIG. 10. (a) Coordinations of nearest-neighbor Eu sites around a Co site. The arrows on the Eu atoms indicate the ordered magnetic moments. (b) Top view of the coordination of nearest-neighbor Eu sites around the Co site. The magnetic moment turn angle between adjacent magnetic layers is ϕ.

direct evidence of the planar incommensurate helix AFM state in $EuCo_2P_2$. Furthermore, using Eq. (3), we can determine the AFM propagation vector $\mathbf{k} = (0,0,k)2\pi/c$, where c is the c-axis lattice parameter of the body-centered tetragonal Eu sublattice. Since the distance d along the c axis between adjacent layers of FM-aligned Eu moments is $d = c/2$, the turn angle between the ordered moments in adjacent Eu layers is $\phi = kd$, as shown in Fig. 10(b). Using $\langle\mu\rangle = 6.9(1)\mu_{\rm B}$ [4], $A^{\rm Co} = -0.98(9)$ kOe/$\mu_{\rm B}$ per Eu, and $B_{\rm int}^{\rm Co} = 11.3(1)$ kOe, the turn angle ϕ is estimated to be $131^\circ \pm 16^\circ$, corresponding to a helix wave vector $\mathbf{k} = (0,0,0.73 \pm 0.09)2\pi/c$. This value of $\mathbf{k}$ is slightly smaller than $\mathbf{k} = (0,0,0.852)2\pi/c$ obtained from the ND data [4] and $(0,0,0.88)2\pi/c$ estimated from the χ data [9] on $EuCo_2P_2$ and is close to $\mathbf{k} = (0,0,0.73)2\pi/c$ determined from the NMR data in $EuCo_2As_2$ [3]. The origin of the small difference in $\mathbf{k}$ between the NMR and ND (and χ) data is not clear, but it could be explained, e.g., if one were to take other small contributions to the hyperfine field at the Co site from the NNN Eu spins.

The asymmetric shape of the observed ^{59}Co ZFNMR spectrum originates from a distribution of the internal field at the Co sites. The ^{153}Eu ZFNMR lines are sharp, as seen in Fig. 2, indicating homogeneous Eu ordered moments. The very sharp ^{31}P ZFNMR line also indicates that the direction of the Eu moments in each ferromagnetic Eu plane is relatively uniform. Therefore, the low-frequency tail of the Co ZFNMR spectrum suggests a distribution of the turn angle ϕ, i.e., the AFM propagation vector $\mathbf{k}$. Using values of the internal field distribution of the Co site from 0.6 T (6 MHz) to 1.2 T (12 MHz), the distribution of the turn angle ϕ is estimated to be from 156° to 131°. This corresponds to a change in $\mathbf{k}$ from $(0,0,0.86)2\pi/c$ to $(0,0,0.73)2\pi/c$. It is worth mentioning that the NMR technique determines not only the AFM propagation vector but also its distribution.

Finally, we discuss the temperature dependence of the turn angle ϕ. Assuming the temperature dependence of the Eu ordered moments $\langle\mu\rangle$ is described by the temperature dependence of $B_{\rm int}^{\rm P}$, one can estimate ϕ at each temperature based on the temperature dependence of $B_{\rm int}^{\rm Co}$ using Eq. (3). As shown in the inset of Fig. 9, ϕ is nearly independent of temperature up to 30 K. According to the ND measurements, on the other hand, ϕ changes from 150° at 64 K just below $T_{\rm N}$ to 153° at 15 K [4]. Thus, the small 2% change in ϕ observed in the ND measurements may occur at temperatures higher than 30 K.

IV. SUMMARY AND CONCLUDING REMARKS

We have carried out ^{153}Eu, ^{31}P, and ^{59}Co NMR measurements on the helical antiferromagnet $EuCo_2P_2$ with $T_{\rm N} = 66.5$ K. The external magnetic field dependence of ^{153}Eu and ^{31}P NMR spectra for single-crystalline $EuCo_2P_2$ clearly evidenced the incommensurate helical AFM structure. The AFM propagation vector characterizing the incommensurate helical AFM state was determined to be $\mathbf{k} = (0,0,0.73 \pm 0.09)2\pi/c$ from the internal magnetic induction at the Co site obtained by ^{59}Co NMR under zero magnetic field. The AFM propagation vector is revealed to be nearly independent of temperature up to 30 K, indicating that the small change in the propagation vector observed by ND measurements may occur at temperatures higher than 30 K.

As described in [3], our NMR approach can be used to study in detail the magnetism originating from the Eu spins in the Co-substituted iron pnictide high-T_c superconductor $Eu(Fe_{1-x}Co_x)_2As_2$. The $x = 0$ compound, $EuFe_2As_2$, exhibits the stripe-type AFM order at 186 K due to the Fe spins. At the same time, the Eu^{2+} moments order antiferromagnetically below 19 K with the A-type AFM structure where the Eu ordered moments are FM aligned in the ab plane but the moments in adjacent layers along the c axis are antiferromagnetically aligned [19]. With substitution of Co for Fe in $Eu(Fe_{1-x}Co_x)_2As_2$, the magnetic structure of the Eu^{2+} spins changes from the A-type AFM order in the $x = 0$ compound to the A-type canted AFM structure at intermediate Co doping levels around $x \sim 0.1$ and then to the FM order along the c axis at $x \sim 0.18$, where superconductivity (SC) appears below $T_c \sim 10$ K in the range $x = 0.1$ to 0.18 [20]. Thus, it is important to understand the magnetism originating from the Eu and Fe spins and also the SC properties from a microscopic point of view. Our approach based on the NMR technique provides an important avenue to study the origin of the coexistence of SC and magnetism in $Eu(Fe_{1-x}Co_x)_2As_2$ SCs.

ACKNOWLEDGMENTS

We thank H. Uehara and F. Kubota for assistance with the experiments. The research was supported by the U.S. Department of Energy, Office of Basic Energy Sciences, Division of Materials Sciences and Engineering. Ames Laboratory is operated for the U.S. Department of Energy by Iowa State University under Contract No. DE-AC02-07CH11358. Part of the work was supported by the Japan Society for the Promotion of Science KAKENHI: J-Physics (Grants No. JP15K21732, No. JP15H05885, and No. JP16H01078). N.H. also thanks the KAKENHI: J-Physics for financial support to be a visiting scholar at Ames Laboratory.

[1] C. Lacroix, P. Mendels, and F. Mila, *Introduction to Frustrated Magnetism*, Springer Series in Solid-State Sciences Vol. 164 (Springer, New York, 2011).

[2] *Frustrated Spin Systems*, edited by H. T. Diep (World Scientific, Singapore, 2005).

[3] Q.-P. Ding, N. Higa, N. S. Sangeetha, D. C. Johnston, and Y. Furukawa, NMR determination of an incommensurate helical antiferromagnetic structure in $EuCo_2As_2$, Phys. Rev. B **95**, 184404 (2017).

[4] M. Reehuis, W. Jeitschko, M. H. Möller, and P. J. Brown, A neutron diffraction study of the magnetic structure of $EuCo_2P_2$, J. Phys. Chem. Solids **53**, 687 (1992).

[5] V. K. Anand and D. C. Johnston, Antiferromagnetism in $EuCu_2As_2$ and $EuCu_{1.82}Sb_2$, Phys. Rev. B **91**, 184403 (2015).

[6] R. Marchand and W. Jeitschko, Ternary lanthanoid-transition metal pnictides with $ThCr_2Si_2$-type structure, J. Solid State Chem. **24**, 351 (1978).

[7] E. Mörsen, B. D. Mosel, W. Müller-Warmuth, M. Reehuis, and W. Jeitschko, Mössbauer and magnetic susceptibility investigations of strontium, lanthanum and europium transition metal phosphides with $ThCr_2Si_2$ type structure, J. Phys. Chem. Solids **49**, 785 (1988).

[8] T. Nakama, T. Yoshida, A. Ohno, D. Nakamura, Y. Takaesu, M. Hedo, K. Yagasaki, K. Uchima, T. Fujiwara, and T. Shigeoka, Effect of pressure on thermopower and resistivity of $EuCo_2P_2$, J. Phys. Conf. Ser. **200**, 032050 (2010).

[9] N. S. Sangeetha, E. Cuervo-Reyes, A. Pandey, and D. C. Johnston, $EuCo_2P_2$: A model molecular-field helical Heisenberg antiferromagnet, Phys. Rev. B **94**, 014422 (2016).

[10] X. Tan, G. Fabbris, D. Haskel, A. A. Yaroslavtsev, H. Cao, C. M. Thompson, K. Kovnir, A. P. Menushenkov, R. V. Chernikov, V. O. Garlea, and M. Shatruk, A transition from localized to strongly correlated electron behavior and mixed valence driven by physical or chemical pressure in ACo_2As_2 (A = Eu and Ca), J. Am. Chem. Soc. **138**, 2724 (2016).

[11] D. C. Johnston, Magnetic Susceptibility of Collinear and Noncollinear Heisenberg Antiferromagnets, Phys. Rev. Lett. **109**, 077201 (2012).

[12] D. C. Johnston, Unified molecular field theory for collinear and noncollinear Heisenberg antiferromagnets, Phys. Rev. B **91**, 064427 (2015).

[13] R. J. Goetsch, V. K. Anand, and D. C. Johnston, Helical antiferromagnetic ordering in $Lu_{1-x}Sc_xMnSi$, Phys. Rev. B **90**, 064415 (2014).

[14] M. Chefki, M. M. Abd-Elmeguid, H. Micklitz, C. Huhnt, W. Schlabitz, M. Reehuis, and W. Jeitschko, Pressure-Induced Transition of the Sublattice Magnetization in $EuCo_2P_2$: Change from Local Moment Eu($4f$) to Itinerant Co($3d$) Magnetism, Phys. Rev. Lett. **80**, 802 (1998).

[15] C. P. Slichter, *Principles of Magnetic Resonance*, 3rd ed. (Springer, New York, 1990).

[16] M. Yogi, S. Nakamura, N. Higa, H. Niki, Y. Hirose, Y. Onuki, and H. Harima, ^{153}Eu and ^{69,71}Ga zero-field NMR study of antiferromagnetic state in $EuGa_4$, J. Phys. Soc. Jpn. **82**, 103701 (2013).

[17] A. J. Freeman and R. E. Watson, Hyperfine interactions in magnetic materials, in *Magnetism*, edited by G. T. Rado and H. Suhl (Academic, New York, 1965), Vol. 2A, Chap. 4, pp. 167–305.

[18] D. C. Johnston, Magnetic dipole interactions in crystals, Phys. Rev. B **93**, 014421 (2016).

[19] H. S. Jeevan, Z. Hossain, D. Kasinathan, H. Rosner, C. Geibel, and P. Gegenwart, Electrical resistivity and specific heat of single-crystalline $EuFe_2As_2$: A magnetic homologue of $SrFe_2As_2$, Phys. Rev. B **78**, 052502 (2008).

[20] W. T. Jin, Y. Xiao, Z. Bukowski, Y. Su, S. Nandi, A. P. Sazonov, M. Meven, O. Zaharko, S. Demirdis, K. Nemkovski, K. Schmalzl, L. M. Tran, Z. Guguchia, E. Feng, Z. Fu, and Th. Brückel, Phase diagram of Eu magnetic ordering in Sn-flux-grown $Eu(Fe_{1-x}Co_x)_2As_2$ single crystals, Phys. Rev. B **94**, 184513 (2016).